Compressive Response of Concrete Confined with Steel Spirals and FRP Composites

J.-Y. LEE,[1] C.-K. YI,[2,]* H.-S. JEONG,[3] S.-W. KIM[4] AND J.-K. KIM[1]

[1]*Department of Architectural Engineering, Sungkyunkwan University 300, Chunchun-dong, Jangan-gu, Suwon 440-746, Republic of Korea*

[2]*School of Civil, Environmental, and Architectural Engineering Korea University, Anam-dong, Seongbuk-gu, Seoul 136-713, Republic of Korea*

[3]*Construction Engineering Service Network Co., 833-2 Yeoksam-dong Kangnam-gu, Seoul 135-933, Republic of Korea*

[4]*Department of Architectural Engineering, Kongju National University 275 Budae-dong, Cheonan 330-717, Republic of Korea*

ABSTRACT: This article presents the results of an experimental and analytical study on the behavior of concrete cylinders externally wrapped with fiber-reinforced polymer (FRP) composites and internally reinforced with steel spirals. The experimental work was carried out by testing twenty-four $150 \times 300\,\text{mm}^2$ concrete cylinders subjected to pure compression with various confinement ratios and types of confining material. The test results show that the compressive response of concrete confined with both FRP and steel spirals cannot be predicted by summing the individual confinement effects obtained from FRP and steel spirals. This is largely attributable to differences in the inherent material properties of FRP and steel. A new empirical model to predict the axial stress–strain behavior of concrete confined with FRP and steel spirals is proposed. Comparisons between experimental results and theoretic predictions show agreement.

KEY WORDS: fiber-reinforced polymer, lateral confining pressure, confined concrete, steel spiral, deformability, concrete cylinder.

INTRODUCTION

IN THE LAST two decades, the use of fiber-reinforced polymer (FRP) composites has drawn much attention in the civil engineering community, which faces stringent new design requirements and demands for lower cost [1]. FRP has proven itself as the material of choice to meet these new needs with its many favorable properties, such as a high strength-to-weight ratio, effective corrosion resistance, and ease of on-site handling and

*Author to whom correspondence should be addressed. E-mail: chongku@korea.ac.kr

0021-9983/10/04 0481–24 $10.00/0 DOI: 10.1177/0021998309347568

application in confined spaces resulting in reduced labor costs. It has been demonstrated that lateral confinement increases compression strength, deformability, and energy absorption capacity of concrete [2,3]. Effective lateral confinement can be achieved by wrapping FRP composite around the perimeter of a concrete member.

Early attempts to use FRP composites as confining materials in columns were performed by Kurt [4] and Fardis and Khalili [5,6]. These attempts were followed by many experimental studies to investigate the effects of FRP spirals [7,8], FRP wraps [9–19], and FRP tubes [20–23] on the compressive response of concrete columns. The early analytical model used to predict the compressive response of concrete confined with FRP composites closely follows the models derived for steel confinements (spirals, hoops, or ties) [24]. However, such models yield inaccurate and often unconservative results [25]. Improved mathematical models have been proposed to capture FRP and concrete material behaviors and to predict the compressive response of concrete confined with FRP composites [26–28].

Most of the previous experimental and analytical studies focus on the compressive response of concrete confined with either FRP composites or steel spirals. In reality, when reinforced concrete (RC) columns are wrapped with FRP composites, the core concrete is confined simultaneously by two different confining materials as follows: the FRP composites and the steel reinforcements already present in the column, as shown in Figure 1(a) [29]. If both confining materials are similar in their stress–strain behaviors, then the compressive response of concrete confined with the two materials (e.g., steel spirals and FRP composites) can be predicted using the models developed for a single confining material with the equivalent confinement ratio of the external and internal reinforcements. However, the stress–strain behavior of steel is quite different from that of FRP composites.

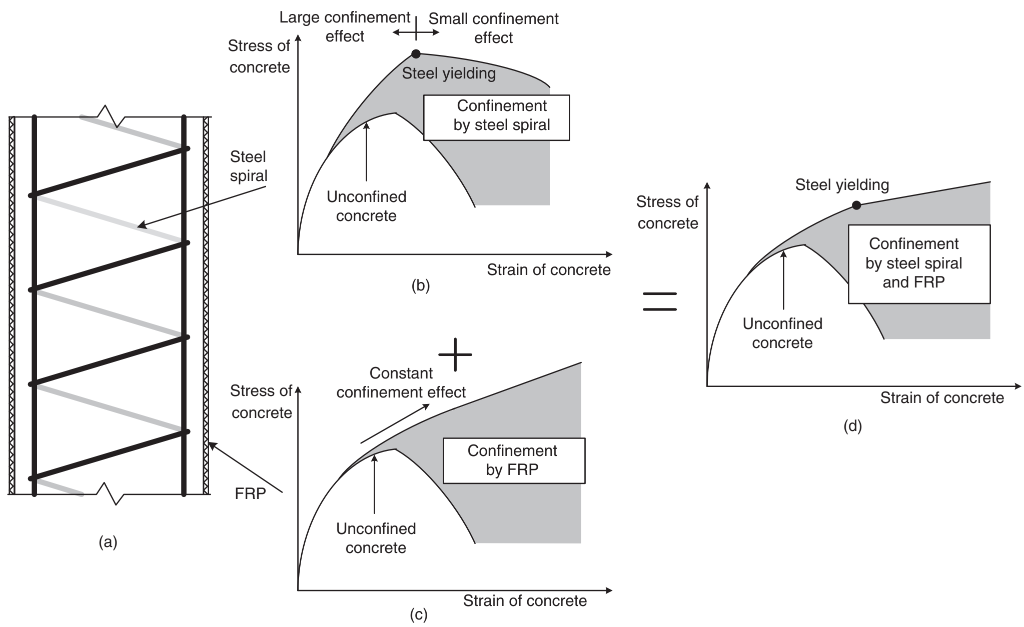

Figure 1. *Compressive response of concrete confined by various materials: (a) concrete column, (b) stress–strain curve of concrete confined by steel spiral, (c) stress–strain curve of concrete confined by FRP, and (d) stress–strain curve of concrete confined by both steel spiral and FRP.*

The stress–strain curve of steel exhibits an initial linear-elastic stage followed by a yielding plateau, in which the tensile strain increases with little increase in stress. In contrast, the tensile stress–strain curve of FRP composites remains linear elastic until the final brittle rupture. Figure 1(b) and (c) depict the compressive stress–strain curves of steel spiral-confined concrete and FRP-confined concrete, respectively, and clearly demonstrate the differences between their behaviors. The compressive stress–strain curve of concrete confined with steel spirals shows loss of stiffness before it reaches its maximum strength, after which the compressive response follows a gradual post-peak descending branch, and the failure strength is typically lower than the peak strength. On the other hand, the compressive stress–strain curve of FRP-confined concrete presents a nearly bilinear response, as shown in Figure 1(c). Therefore, when concrete is confined by these two materials, a link between the confinement effects of the different materials must be established.

The confinement effect of different material was also investigated by Liu et al. [30] who tested concrete columns to investigate the confinement effect of fiber-reinforced composites fabricated by filament winding method with various combinations of hybrid fibers and lay up angles on the compressive strengths of concrete. According to Liu et al.'s test results, the compressive strengths of concrete columns were influenced by the combination of hybrid fibers. For example, concrete columns confined by the foil-glass–Kevlar-glass (FGKG) hybrid composites were stronger than those reinforced by the foil-glass–carbon-glass (FGCG) hybrid composites. However, Liu et al.'s hybrid fibers were resin cured and essentially became a single confining composite material around the concrete cylinder before the compressive test; hence, the analysis of the effect of each fiber type on the concrete compressive behavior was limited.

This article presents the results of an experimental and analytical study on the performance of concrete cylinders externally wrapped with FRP sheets and internally reinforced with steel spirals. Twenty-four $150 \times 300\,\mathrm{mm}^2$ concrete cylinders are tested under pure compression. Applied load, axial strain, and lateral strain are recorded to monitor the stress–strain behavior, ultimate strength, and corresponding strain of the tested specimens. The experimental results are then compared with some of the existing confinement models available in the technical literature. In addition, a new analytical model to predict the behavior of concrete confined with both FRP and steel is proposed.

TEST PROGRAM

Test Specimens

A total of twenty-four $150 \times 300\,\mathrm{mm}^2$ cylindrical specimens were prepared from the same concrete mix. The cylinders were divided into four series with four different steel confinement ratios ($\rho_{ls} = 4A_{sp}/(d_s \cdot s)$, where A_{sp} is the cross-sectional area of the steel spiral, s is the pitch of spirals, and d_s is the distance between the centers of the spiral, 130 mm), as given in Table 1 in which the test specimens are designated with two letters, S and F for the steel confinement and the FRP confinement, respectively. The numeric digits following the letters S and F designate the pitch of the steel spiral ties in centimeters and the number of layers of the FRP composite applied, respectively. For example, specimen S0F0 indicates that this cylinder was neither confined with steel spiral hoops nor FRP sheets, while S2F4 indicates that this cylinder was confined with both the steel spiral ties

Table 1. Material properties of specimens.

Specimen	f'_c (MPa)	ε_{c0} (%)	f_{sy} (MPa)	s (mm)	f_{fy} (MPa)	E_{frp} (GPa)	t (mm)	Number of layers
S0F0	36.2	0.24	1200	–	–	–	–	–
S0F1	36.2	0.24	1200	–	4510	250	0.11	1
S0F2	36.2	0.24	1200	–	4510	250	0.22	2
S0F3	36.2	0.24	1200	–	4510	250	0.33	3
S0F4	36.2	0.24	1200	–	4510	250	0.44	4
S0F5	36.2	0.24	1200	–	4510	250	0.55	5
S6F0	36.2	0.24	1200	60	–	–	–	–
S6F1	36.2	0.24	1200	60	4510	250	0.11	1
S6F2	36.2	0.24	1200	60	4510	250	0.22	2
S6F3	36.2	0.24	1200	60	4510	250	0.33	3
S6F4	36.2	0.24	1200	60	4510	250	0.44	4
S6F5	36.2	0.24	1200	60	4510	250	0.55	5
S4F0	36.2	0.24	1200	40	–	–	–	–
S4F1	36.2	0.24	1200	40	4510	250	0.11	1
S4F2	36.2	0.24	1200	40	4510	250	0.22	2
S4F3	36.2	0.24	1200	40	4510	250	0.33	3
S4F4	36.2	0.24	1200	40	4510	250	0.44	4
S4F5	36.2	0.24	1200	40	4510	250	0.55	5
S2F0	36.2	0.24	1200	20	–	–	–	–
S2F1	36.2	0.24	1200	20	4510	250	0.11	1
S2F2	36.2	0.24	1200	20	4510	250	0.22	2
S2F3	36.2	0.24	1200	20	4510	250	0.33	3
S2F4	36.2	0.24	1200	20	4510	250	0.44	4
S2F5	36.2	0.24	1200	20	4510	250	0.55	5

having a pitch of 2 cm and four layers of the FRP composite. The pitch of spirals was varied from 20–60 mm. The steel spirals were made of 5.0 –mm diameter bars and had the yield strength of 1200 MPa. The cross-sectional area of the spiral (A_{sp}) is 19.63 mm^2. Each series consists of six cylinders, each with a different FRP confinement ratio ($\rho_{lf} = 4t/D$, where t is the thickness of the FRP composites and D is the diameter of cylinder). FRP sheets had a thickness of 0.11 mm and a tensile strength of 4500 MPa. The layer of FRP sheets was varied from 0 to 5 (Table 1).

The concrete cylinders were removed from the forms after 24 h. The cylinders were cured at room temperature for 28 days before test. After curing the cylinders, the surfaces of the specimens were cleaned using an electric grinder, and primer was applied to the surfaces of the beams. The FRP sheets were then placed using the epoxy (Epondex by Hankuk Carbon, Inc.) after the primer had completely dried. The carbon FRP composites were formed by embedding continuous fibers in resin matrix (digycidyl ether bisphenol A (DGEBA) epoxy and accelerator of hardening), which binds the fibers together. The poly acrylonitrile (PAN) carbon fiber produced by Toray, Inc. was used in the FRP composites. The FRP sheets were formed by hand lay-up method at room temperature.

The compressive tests of the unconfined concrete cylinder were performed on the first test day of each series, and the four average concrete strengths and corresponding strains were obtained as 36.1, 36.2, 36.1, and 36.4 MPa, and 0.00244, 0.00242, 0.00244, and 0.00239, respectively. Table 1 presents the overall average concrete strength and corresponding strain, and the material properties of the steel spirals and FRP composites.

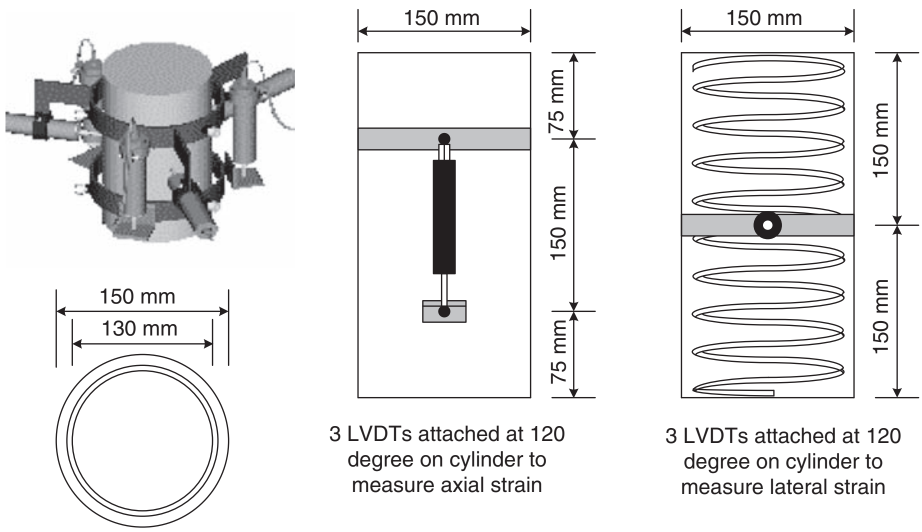

Figure 2. *Specimen geometry, steel layout, and arrangement of LVDTs.*

Measurements

Figure 2 illustrates the overall dimensions and reinforcement layout. Six linear displacement transducers (LVDTs) were attached to the cylinder's surface. Three of the six LVDTs measured the axial deformation, and the remaining three LVDTs were attached horizontally 120° apart at the midheight of each specimen to measure the lateral strains of the specimens. In addition, the strains of the transverse steel reinforcement were recorded using the three strain gages attached on surfaces of the steel spiral prior to the concrete cast.

The axial compression tests were performed using a universal testing machine with a capacity of 2000 kN. The load was applied monotonically until the specimen failed or the load dropped to about 85% of the maximum recorded load in the post-peak descending branch. A data logger (EDX-1500A) recorded the values of the applied load, the axial deformations via the corresponding LVDTs, and the strains. These values were recorded at specified load intervals.

TEST RESULTS

Compressive Axial Stress–Strain Curves

The axial compression stress–strain curves of the 24 RC cylinders are shown in Figure 3(a)–(d), where the test specimens are designated using the same notation as in Table 1. Each series consisted of six cylinders. The test results of specimen S6F3 was not recorded due to errors in the data logger.

It is noted that the stiffness of the unconfined S0F0 specimen and other confined specimens are almost identical in the elastic range, where the axial compressive strain is too small to cause lateral strain sufficient to engage passive confinement by the FRP or the steel spirals. The stress–strain curve of concrete becomes nonlinear with further increases

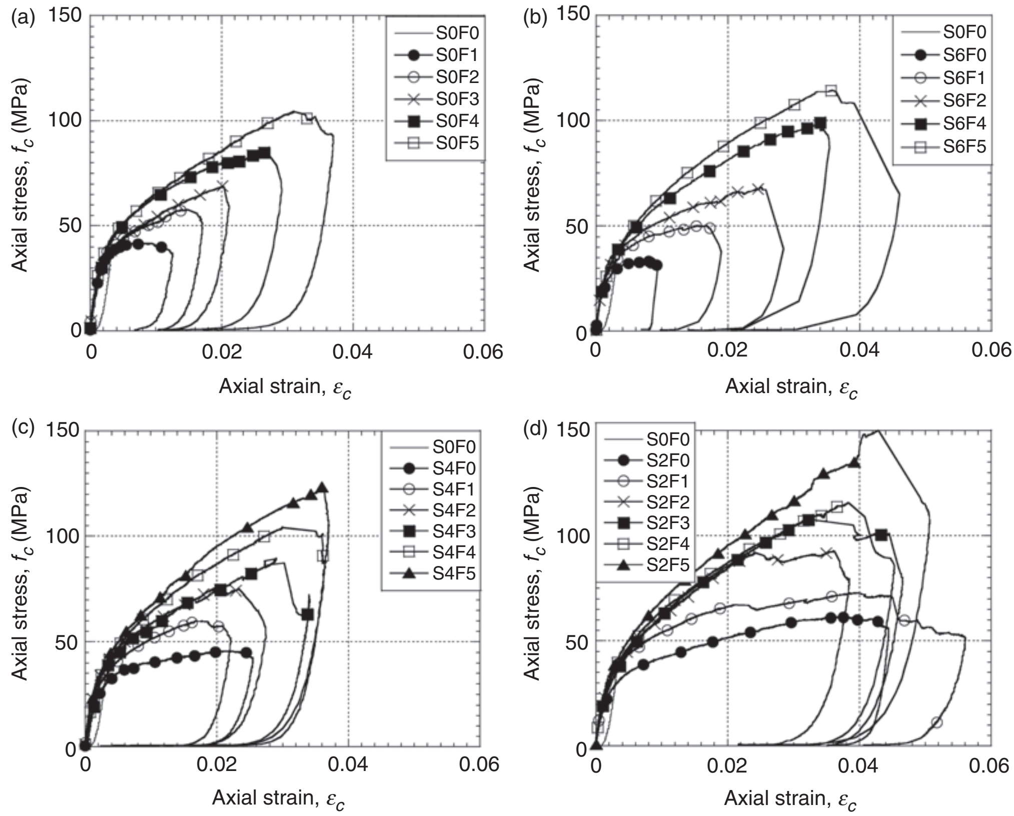

Figure 3. *Compressive axial stress–axial strain curves of tested concrete cylinders: (a) S0 series, (b) S6 series, (c) S4 series, and (d) S2 series.*

in the axial compressive strain, and the strength of concrete increases with the confinement ratio of the FRP and the steel spirals. The typical failure of the specimens confined with both FRP and steel spirals initiated at the midheight of the specimens; none of the test subjects failed due to local fracture of the FRP. The cylinders confined with multilayers of FRP sheets failed suddenly with an explosive noise.

The effect of FRP confinement can be observed in the compressive stress–strain curves of the S0 series in Figure 3(a). The peak stress, the corresponding strain, and the area under the stress–strain curve (energy dissipation capacity) tend to increase with the thickness of the FRP. The comparisons among the stress–strain curves of S6F0, S4F0, and S2F0 (specimens confined only with steel spirals) show a similar trend to that of the FRP confinement. In addition, Figure 3(b)–(d) show that the effects of steel confinement and FRP confinement are additive; as the thickness of the FRP or the volume of the steel spiral increases, the confined concrete exhibits higher strength and greater ductility.

To quantify the effect of the individual confining material (steel spiral or FRP composites) on the compressive behavior of the confined concrete, the lateral confining pressures of steel spirals and FRP wraps (denoted by f_{ls} and f_{lf}, respectively) are considered. The effective lateral confining pressure of steel spirals and FRP wraps for cylindrical

Table 2. Lateral confining pressure, compressive axial strength, and corresponding axial strain of the tested concrete cylinders.

Specimen	f_{ls} (MPa)	f_{lf} (MPa)	f_{cu} (MPa)	ε_{cu}	f_{cu}/f'_c	$\varepsilon_{cu}/\varepsilon_{c0}$
S0F0	0.00	0.00	36.2	0.0024	1.00	1.00
S0F1	0.00	6.61	41.7	0.010	1.15	4.17
S0F2	0.00	13.22	57.8	0.015	1.60	6.25
S0F3	0.00	19.83	69.1	0.020	1.91	8.33
S0F4	0.00	26.44	85.4	0.027	2.36	11.25
S0F5	0.00	33.05	104.3	0.031	2.88	12.92
S6F0	6.04	0.00	33.57	0.008	0.93	3.33
S6F1	6.04	6.61	50.37	0.017	1.39	7.08
S6F2	6.04	13.22	68.52	0.025	1.89	10.42
S6F4	6.04	26.44	99.49	0.034	2.75	14.17
S6F5	6.04	33.05	114.64	0.036	3.17	15.00
S4F0	9.06	0.00	45.77	0.022	1.26	9.17
S4F1	9.06	6.61	60.00	0.019	1.66	7.92
S4F2	9.06	13.22	74.77	0.023	2.07	9.58
S4F3	9.06	19.83	88.80	0.029	2.45	12.08
S4F4	9.06	26.44	104.15	0.030	2.88	12.50
S4F5	9.06	33.05	123.64	0.036	3.42	15.00
S2F0	18.12	0.00	61.50	0.038	1.70	15.83
S2F1	18.12	6.61	72.87	0.039	2.01	16.25
S2F2	18.12	13.22	92.68	0.036	2.56	15.00
S2F3	18.12	19.83	108.01	0.034	2.98	14.17
S2F4	18.12	26.44	115.72	0.038	3.20	15.83
S2F5	18.12	33.05	150.80	0.043	4.17	17.92

members can be estimated using Equation (1) [32] and Equation (2) [34], respectively, for the specimens tested in this study.

$$f_{ls} = \frac{2A_{sp}f_{sy}}{d_s s} \tag{1}$$

$$f_{lf} = \frac{2f_{fy}t}{D}, \tag{2}$$

where A_{sp} is the cross-sectional area of the steel spiral, d_s is the distance between the centers of the spiral, s is the pitch of spirals, f_{sy} is the yield strength of steel spiral, D is the diameter of the concrete cylinder, f_{fy} is the strength of the FRP sheet, and t is the thickness of the FRP. Table 2 gives the values of f_{ls} and f_{lf} for all 24 cylinders computed using Equations (1) and (2), respectively. Table 2 also lists the observed values of the compressive strength, f_{cu}, and the corresponding axial strain, ε_{cu}, of the test cylinders. In addition, the ratio of the maximum compressive stress of each cylinder to that of the control specimen S0F0 as well as the ratio of the compressive strain at the peak stress of each specimen to that of S0F0 is calculated for comparison purposes.

Compressive Strength and Corresponding Axial Strain

The effect of the confining pressure on the compressive strength and corresponding axial strain of concrete is presented in Figure 4(a) and (b). The figures display the variation of the peak concrete compressive stress and corresponding axial strain as a function of the confinement pressure, f_{lf}, provided by the FRP compoistes for each series. For a given steel spiral confining pressure, f_{ls}, the concrete compressive strength, f_{cu}, increases almost linearly when FRP confinement pressure increases as expected. Furthermore, it is noted that the lines representing the four series are almost parallel to one another. These observations suggest that the increments of compressive strength due to FRP and steel confinements are additive and may be expressed as a function of two independent variables, f_{lf} and f_{ls}.

While a linear trend between f_{cu} and f_{lf} for a given f_{ls} is noted in Figure 4(a), the axial compressive strain at the peak stress, ε_{cu}, lacks such a clear relation. Although ε_{cu} increases

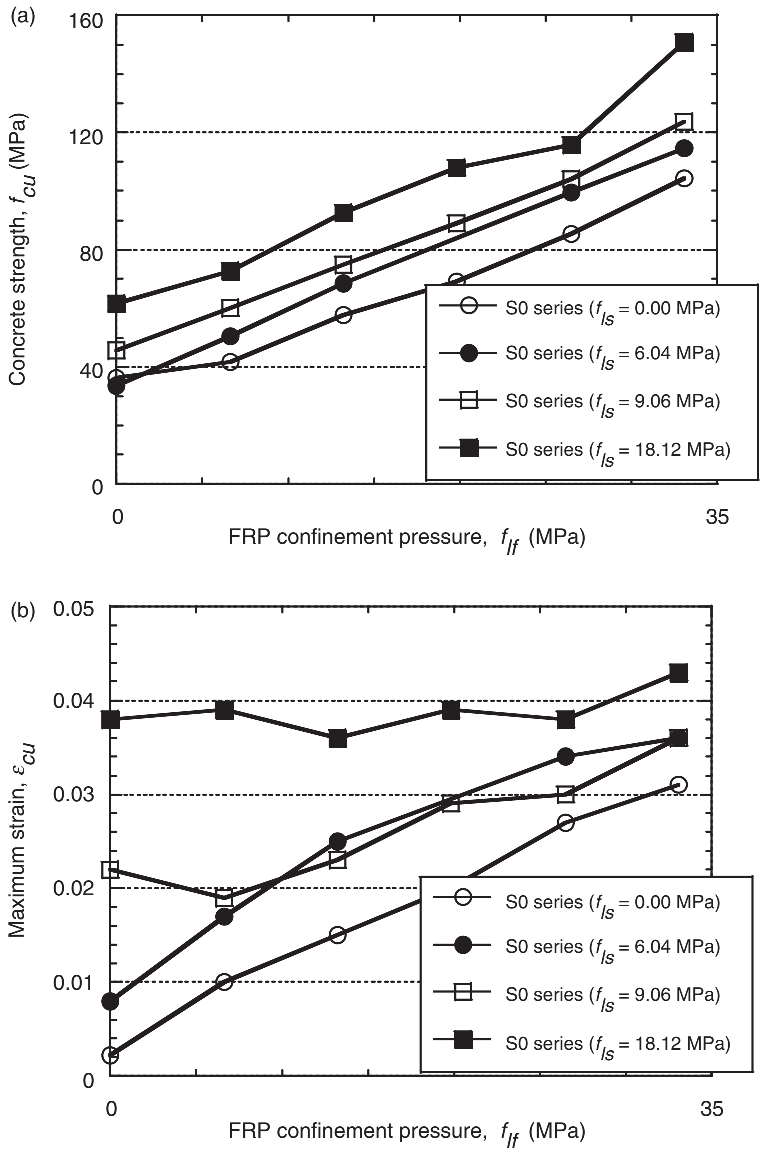

Figure 4. *Peak compressive axial stress and corresponding axial strain: (a) peak compressive strength vs. FRP confinement pressure and (b) corresponding axial strain vs. FRP confinement pressure.*

with FRP confinement pressure in the S0, S6, and S4 series, ε_{cu} remains almost constant in the S2 series. The graph also shows that the slope of the line flattens with higher f_{ls}. These observations indicate that the effects of f_{lf} and f_{ls} on ε_{cu} are not independent of each other. Thus, the weight of the contribution from each confining material to ε_{cu} may vary depending on the relative amount of the confining material or the strain range of interest. A simple analytical model will be presented in a later section.

Compressive Axial Stress–Lateral Strain Curves

Figure 5(a)–(d) display the axial compressive stress vs. the lateral strain of the test specimens. Each figure shows the stress–strain curves of each series. Similar to what is seen in the axial stress–strain curves in Figure 3, two distinct stages are observed in all of the stress–lateral strain curves as follows: a steep initial stage where the concrete compressive axial stress is still less or equal to the unconfined concrete strength (i.e., the strength of cylinder S0F0 in this investigation), and a second stage where the concrete compressive axial stress of the confined cylinders exceeds the unconfined concrete strength of S0F0. The initial slopes of the curves share a similar steepness, though the slopes of the second stage increase as the amount of confinement increases. In other words, the slope of the second stage depends on the lateral confining pressure.

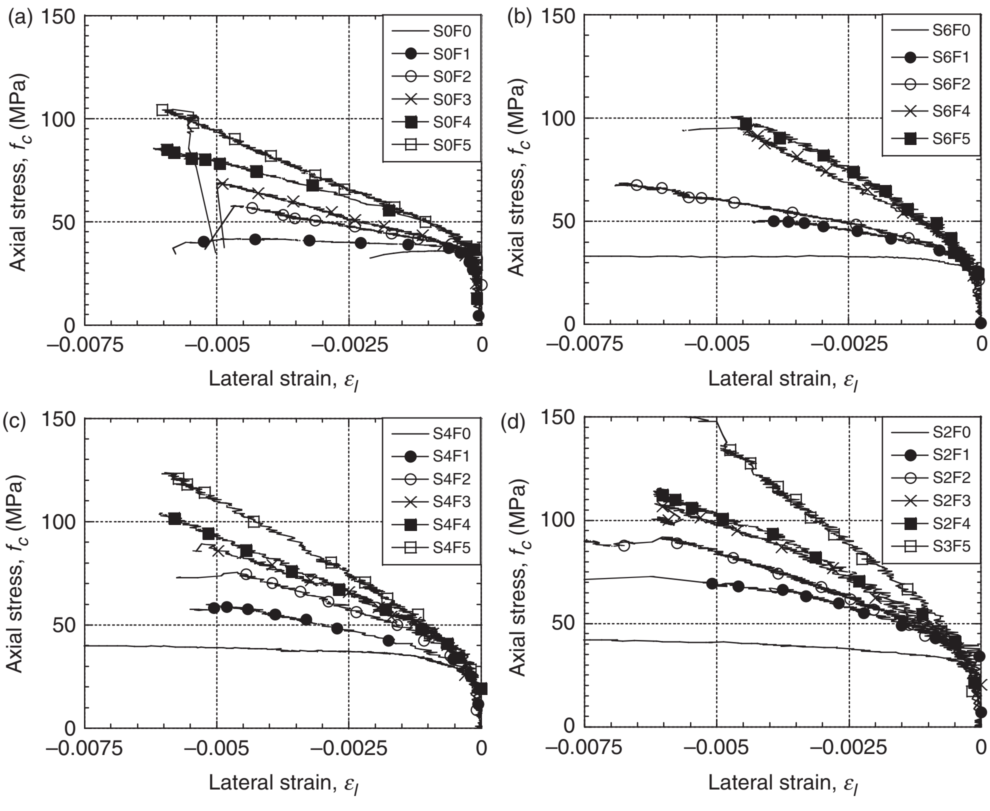

Figure 5. *Compressive axial stress–lateral strain curves of tested concrete cylinders: (a) S0 series, (b) S6 series, (c) S4 series, and (d) S2 series.*

It is noted that the maximum lateral strain of the test cylinders (approximately 0.01) is smaller than a typical rupture strain of carbon fiber reinforced polymer (0.015 based on flat coupon tensile tests). The difference between the FRP rupture tensile strain from material tests and that obtained in FRP-confined concrete specimens is explained by Lam and Teng [31], who attribute the difference to the following three factors: (1) the curvature of the FRP jacket, (2) the nonuniform deformation of cracked concrete, and (3) the existence of an overlapping zone. The maximum strain (about 0.01) observed in this study agrees with the value reported by Lam and Teng.

EFFECTS OF CONFINEMENT ON THE COMPRESSIVE RESPONSE OF CONCRETE

Compressive Stress–Strain Curves of Concrete

The test results of two pairs of specimens (S0F4 and S2F1, and S0F3 and S6F2) are examined carefully to study the effect of the confinement type (FRP vs. steel spirals) on the compressive axial stress–strain curves of concrete. The specimens in each pair are chosen so that the two specimens have similar total confining pressure as determined by Equations (1) and (2).

Figure 6(a) shows the compressive stress–strain curves of specimens S0F4 and S2F1. Specimen S0F4 was confined with only four layers of FRP sheets, while S2F1 was confined with one layer of FRP and steel spirals at a pitch of 20 mm. The total confining pressures ($f_{ls} + f_{lf}$) of S0F4 and S2F1 are 26.44 and 24.73 MPa, respectively. Similarly, Figure 6(b) shows the stress–strain curves of specimens S0F3 and S6F2 with a total confining pressure of about 19 MPa. Figure 6(a) and (b) show that even under the same total confining pressure, concrete can exhibit very different compressive behaviors in terms of deformability and energy dissipation capacity depending on the relative amounts of each confinement material.

Maximum Strain of Concrete

The normalized concrete strain at the peak stress vs. the total confining pressure for all test cylinders is shown in Figure 7(a). The normalized concrete strain was calculated by dividing the concrete strain of each specimen corresponding to the maximum concrete stress by that of the control specimen S0F0. In general, the normalized strains show a linear relation with respect to the total confining pressure as long as the pitch of the steel spiral is less than 40 mm. The ineffectiveness of increasing confinement pressure becomes clear when the pitch of the steel spiral is 20 mm, as shown in Figure 7(b). Although the total confining pressure of cylinder S2F4 is equal to the sum of the confining pressures of cylinders S2F0 and S0F4, the strain corresponding to the peak compressive stress of cylinder S2F4 is far less than the sum of the peak strains of cylinders S2F0 and S0F4. In fact, ε_{cu} of S2F4 is about equal to that of cylinder S2F0 (Table 2). The conclusion that the effect of FRP confinement on ε_{cu} is negligible may be presumptuous when there exists a substantial confinement by steel spiral or hoop, though the test results clearly indicate that the effect of FRP confinement on ε_{cu} gets overshadowed as steel confinements increase. This observation may be utilized to develop an analytical model to predict the value of ε_{cu} of the concrete with mixed confinement materials.

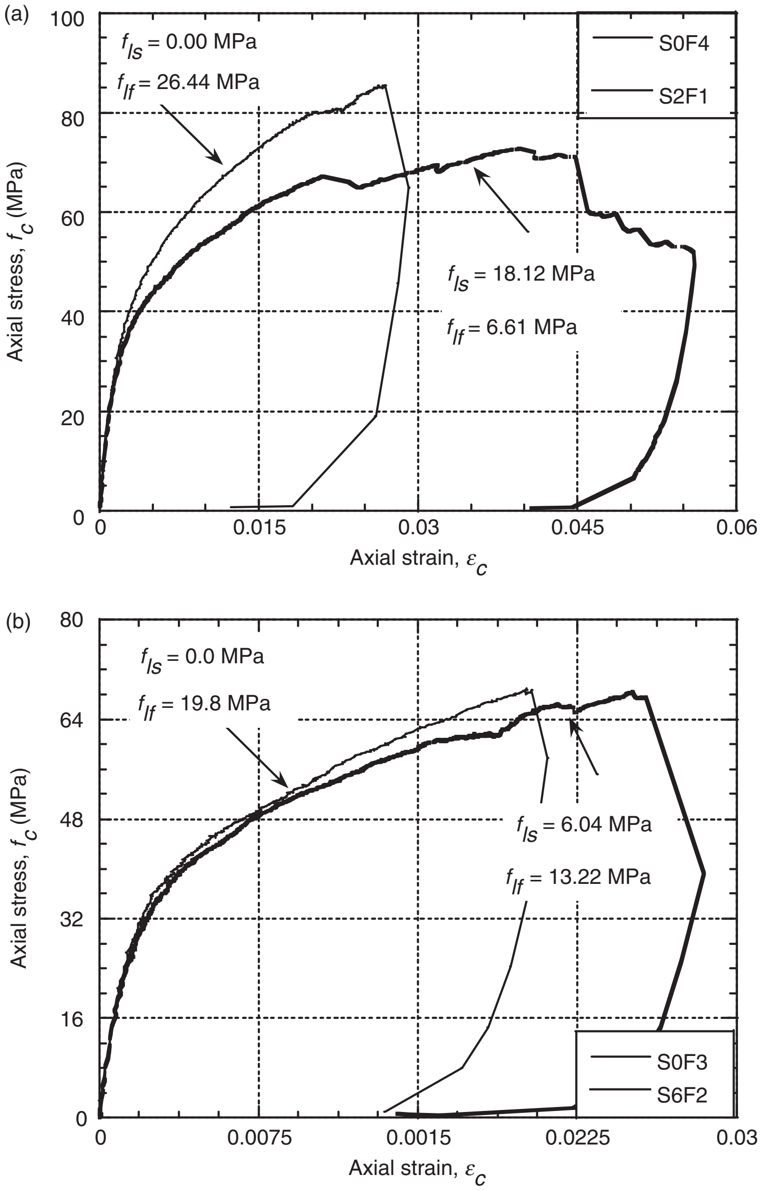

Figure 6. *Comparison of the experimental axial stress–axial strain curves of tested cylinders: (a) S0F4 and S2F1, and (b) S0F3 and S6F2.*

Compressive Strength of Concrete

Figure 8(a) shows the normalized strength of concrete, which is the ratio of the concrete strength (f_{cu}) to the concrete strength (f'_c) of specimen S0F0, vs. the total confining pressure $f_{ls} + f_{lf}$ of each specimen. The value of f_{cu} increases linearly with the total confining pressure up to 50 MPa, which is the maximum confining pressure considered in this study.

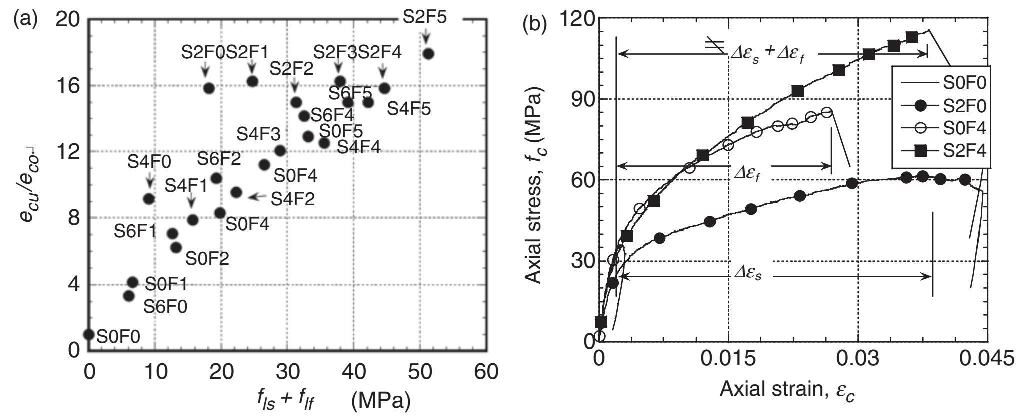

Figure 7. *Effects of confinement on the maximum strain of concrete: (a) maximum strain vs. confining pressure and (b) comparison of the axial stress–axial strain of tested cylinders, S0F0, S2F0, S0F4, and S2F4.*

The additive characteristics of strength enhancements from the different confining materials can also be seen in Figure 8(b), which shows the compression stress–strain curves of four specimens as follows: S0F0, S4F0, S0F4, and S4F4. The difference in strength between S4F0 and S0F0 is denoted by Δf_s, and the increase in strength between S0F4 and S0F0 is denoted by Δf_f. Unlike the behavior that is observed in ε_{cu}, the strength of S4F4 (which is wrapped with four layers of FRP composites and reinforced with steel spirals at a 40 mm pitch) is equivalent to the sum of Δf_s (S4F0) and Δf_f (S0F4). This observation suggests that the FRP and steel spiral retain their own contributions to the total strength enhancement until the failure occurs (i.e., $\Delta f_{s+f} = \Delta f_s + \Delta f_f$).

PREDICTING THE RESPONSE OF CONFINED CONCRETE

The experimental results of this investigation are compared with the predicted values given by some of the existing confinement models available in the technical literature. It is noted that the four existing models are originally derived for a concrete confined by a single material. Therefore, the comparison study was carried out to identify ways to modify the existing models rather than to test their accuracy. Upon identifying the deviation of the existing models, a new prediction model for concrete confined with both steel spirals and FRP wrap was proposed.

Four models by Mander et al. [32], Samman et al. [33], Lam and Teng [34], and Saafi et al. [21] are considered in this study for their easy-to-use equations and robustness. The model developed by Mander et al. is based on the works by Popovics [35] and Elwi and Murray [36] using the energy balance approach for steel confinement. The model is widely accepted and adopted by many design codes. Upon the introduction of FRP composites as confining and strengthening materials for columns and beams, an attempt was made to simply extend Mander's model to estimate stress–strain behavior of FRP confined concrete [24,25]. Saafi et al. [21] improved the model by introducing the new confinement effectiveness coefficients to Mander's model and showed reasonable predictions for the FRP tube-confined concrete. Samman et al. [33] and Lam and Teng [34] also developed new models with emphasis on the correlation between the lateral strain and

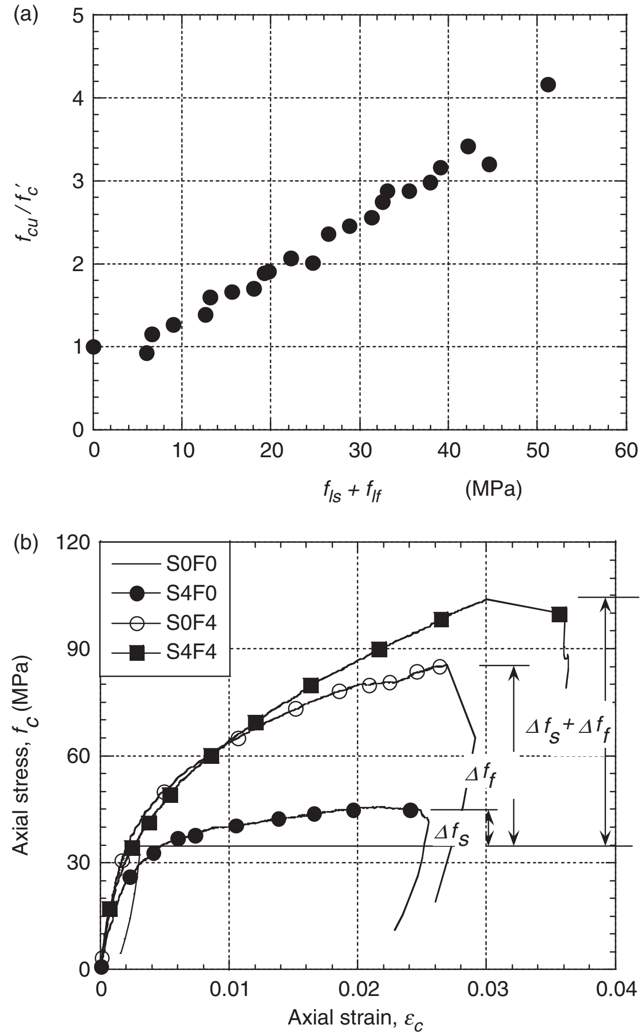

Figure 8. *Effects of confinement on the compressive strength of concrete: (a) compressive strength vs. confining pressure and (b) comparison of the axial stress–axial strain of tested cylinders, S0F0, S4F0, S0F4, and S4F4.*

hoop stiffness of the FRP. Detailed equations from the four analytical models are tabulated in Table 3.

Existing Analytical Models

In determining the stress–strain curves, Equation (3) is used to estimate the compressive stress because the core concrete and the cover concrete are subject to different confining pressures.

$$f_c = (f_{c-\text{core}} A_{\text{core}} + f_{c-\text{cover}} A_{\text{cover}})/A_g, \tag{3}$$

Table 3. Existing analytical models to predict the compressive behavior of confined concrete.

Model	Stress–strain relationship	Parameters
Mander et al.	$f_c = (f_{cu} \cdot x \cdot r)/(r - 1 + x^r)$	$x = \varepsilon_c/\varepsilon_{cu}$
	$f_{cu} = f'_c\left(-1.254 + 2.254\sqrt{1 + 7.94\frac{f_l}{f'_c}} - 2\frac{f_l}{f'_c}\right)$	$r = E_c/(E_c - E_{2m})$
	$\varepsilon_{cu} = \varepsilon_{co}\left(1 + 5\left(\frac{f_{cu}}{f'_c} - 1\right)\right)$	$E_{2m} = f_{cu}/\varepsilon_{cu}$
		$E_c = 5000\sqrt{f'_c}$
		$f_l = \frac{2A_{sp} f_{sy}}{d_s s}$
Mirmiran et al.	$f_c = \frac{(E_c - E_2)\varepsilon_c}{\{1 + [(E_c - E_2)\varepsilon_c/f_o]^n\}^{1/n}} + E_2\varepsilon_c$	$E_c = 3950\sqrt{f'_c}$, $n = 1.5$, $f_l = \frac{2f_{fy}\,t}{D}$
	$f_{cu} = f'_c + 6f_l^{0.7}$, $\varepsilon_{cc} = \frac{f_{cu} - f_0}{E_2}$	$E_2 = 245.61(f'_c)^{0.2} + 1.3456\left(\frac{E_{frp}\,t}{D}\right)$
		$f_o = 0.872f'_c + 0.371f_l + 6.258$
Lam and Teng	$f_c = E_c\varepsilon_c - \frac{(E_c - E_{2l})^2}{4f'_c}(\varepsilon_c)^2$ for $0 \le \varepsilon_c \le \varepsilon_t$	$E_c = 4730\sqrt{f'_c}$
	$f_c = f'_c + E_{2l}\varepsilon_c$ for $\varepsilon_t \le \varepsilon_c \le \varepsilon_{cu}$	$E_{2l} = (f_{cu} - f'_c)/\varepsilon_{cu}$
	$f_{cu} = f'_c\left(1 + 2\frac{f_l}{f'_c}\right)$	$\varepsilon_t = 2f'_c/(E_c - E_{2l})$, $f_l = \frac{2f_{sy}\,t}{D}$
	$\varepsilon_{cu} = \varepsilon_{co}\left(1.75 + 5.53\left(\frac{f_l}{f'_c}\right)\left(\frac{\varepsilon_{frp\,r}}{\varepsilon_{co}}\right)^{0.45}\right)$	
	$f_c = \frac{E_1\varepsilon_c}{1 + \left(\frac{E_c}{f_a} - \frac{2}{\varepsilon_{1a}} + \frac{E_1E_2\varepsilon_{1a}}{f_a^2}\right)\varepsilon_c + \left(\frac{1}{\varepsilon_{1a}^2} - \frac{E_1E_2}{f_a^2}\right)\varepsilon_c^2}$ $0 \le \varepsilon_l \le 0.002$	$f_l(\varepsilon_l) = \frac{2E_{frp}\,t\,\varepsilon_l}{D}$
Saafi et al.	$f_c = f'_c\left(1 + 2.2\left(\frac{f_l(\varepsilon_l)}{f'_c}\right)^{0.84}\right)$ $0.002 \le \varepsilon_l \le \varepsilon_{frp,r}$	$f_a = f'_c\left(1 + 0.0213\left(\frac{E_{frp}\,t}{D\,f'_c}\right)^{0.84}\right)$
	$\varepsilon_c = \varepsilon_{co}\left(1 + (537\varepsilon_l + 2.6)\left(\frac{f_l(\varepsilon_l)}{f'_c} - 1\right)\right)$	$\varepsilon_{1a} = \varepsilon_{co}\left(1 + 0.0783\left(\frac{E_c\,t}{D\,f'_c}\right)^{0.84}\right)$
		$E_1 = 10200\sqrt[3]{f'_c}$, $E_2 = 0.272\frac{f'_c}{\varepsilon_{co}}$

where $f_{c\text{-core}}$ is the core concrete stress confined by both FRP composites and steel spirals, $f_{c\text{-cover}}$ is the cover concrete stress confined only by FRP composites, A_{core} is the area enclosed by the steel spiral per ACI318-08 and A_{cover} is the area of the cross section not enclosed by the steel spiral but enclosed by the FRP composites (i.e., $A_{\text{cover}} = A_{\text{gross}} - A_{\text{core}}$), A_g is the total cross-sectional area of the cylinder. Thus, in deterimining $f_{c\text{-core}}$, the sum of the FRP-confining pressure (f_{lf}) and the steel spiral confining pressure (f_{ls}) is applied as the confining pressure in the models. For $f_{c\text{-cover}}$, only the confining pressure (f_{lf}) is applied.

The predicted compressive stress–strain curves of specimen S2F2 confined with FRP composites and steel spirals are shown in Figure 9. The confining lateral pressures provided by FRP and the steel spirals are 18.1 and 13.2 MPa, respectively. Figure 9(a) and (b) show that some of the existing models predict well the behavior of concrete confined with FRP only (S0F2); however, with the presence of steel spiral in addition to the FRP composites, the same existing models, which accurately predict the behavior of S0F2, tend to either overestimate the peak load or underestimate the strain at peak stress with the presence of steel spirals (S2F2). The weak correlations between the predictions and the experimental results were expected, with regard to mixed confining materials, for which

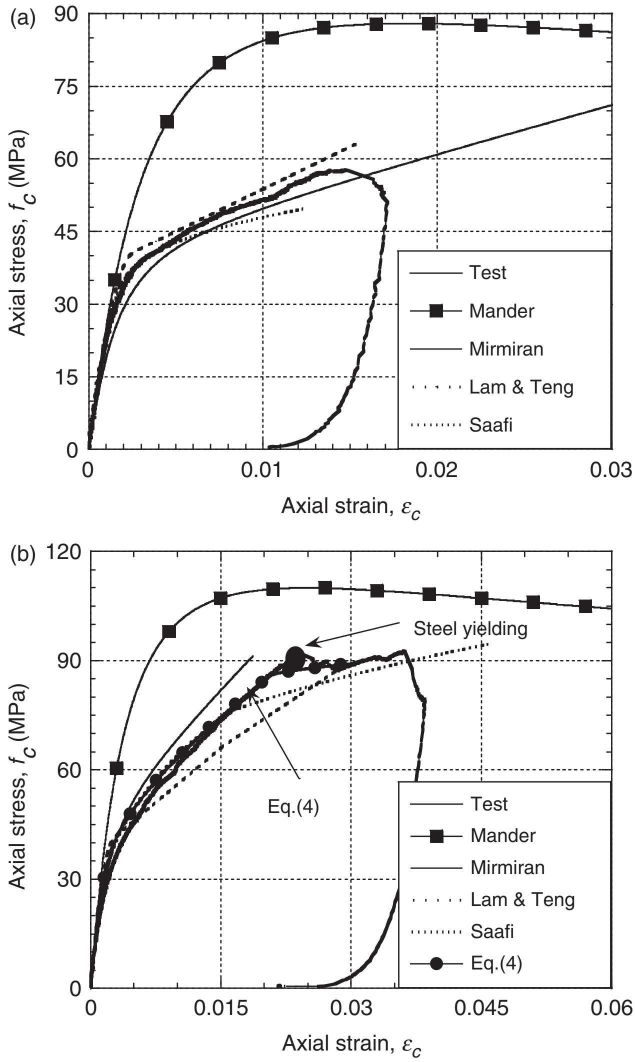

Figure 9. *Comparison between experimental and predicted axial stress–axial strain curves: (a) S0F2 and (b) S2F2.*

stress–strain behaviors differ greatly from each other. This is because the existing models are developed specifically for either FRP or steel stress–strain behavior alone. These results demonstrate that development of a new analytical model is necessary for more accurate estimates of compressive behavior of concrete with the mixed confinement. Figure 10 shows more comparisons between the experimental and predicted stress–strain curves of some of the cylinders in the S2 series. Similar behavior is observed in the S2F2 specimen.

The predicted and experimental strains corresponding to the ultimate confined concrete stresses are also compared. Figure 11(a)–(d) display the ratios of the experimental

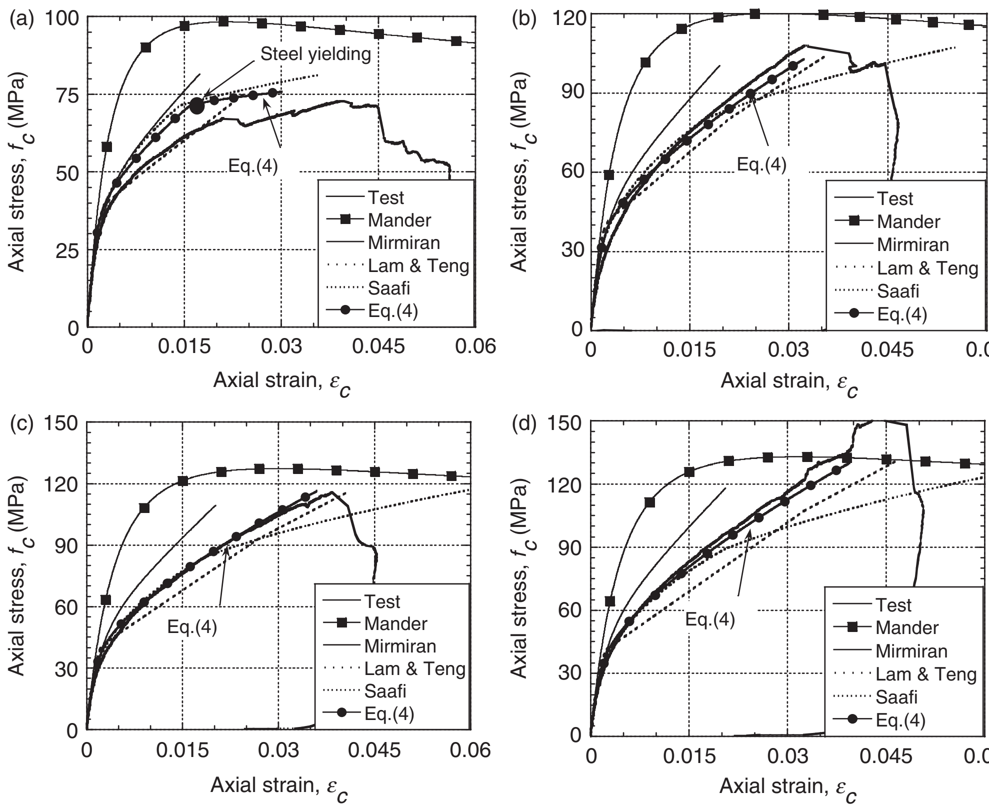

Figure 10. Comparison between experimental and predicted axial stress–axial strain curves of the S2 series: (a) S2F1, (b) S2F3, (c) S2F4, and (d) S2F5.

compressive axial strains at the peak stress to the predicted values ($\varepsilon_{cu-\exp}/\varepsilon_{cu-cal}$) of the 24 tested cylinders. The figures also show the values of the mean, standard deviation, and coefficient of variation (COV) of the strain ratio ($\varepsilon_{cu-\exp}/\varepsilon_{cu-cal}$) of the 24 cylinders. The models by Mander et al. and Lam and Teng tend to slightly overestimate the strain values with mean ratios of 1.23 and 1.14, respectively, and with a similar COV value of approximately 0.3. The other two models show greater scatter in the predicted values with $\varepsilon_{cu-\exp}/\varepsilon_{cu-cal}$ values ranging from 0.25–2.4.

Figure 12 shows the ratios of the experimental ultimate compressive strengths to the predicted strengths of the 24 tested specimens. The mean values of the compressive strength ratios ($f_{cu-\exp}/f_{cu-\mathrm{cal}}$) of the 24 test cylinders calculated by the four models range from 0.80 to 0.96, while the corresponding COV values range from 7.5% to 16.4%. The model by Mander et al. predicts the greatest strength values among the four models, with a mean value of 0.80 and a COV value of 16.4%. The model by Lam and Teng predicts the most accurate strength values, with a mean value of 0.96 and a COV value of 7.5%. The models by Saafi et al. and Mirmiran et al. predict the strength values with slightly greater scatter than those obtained by Mander et al. and Lam et al.

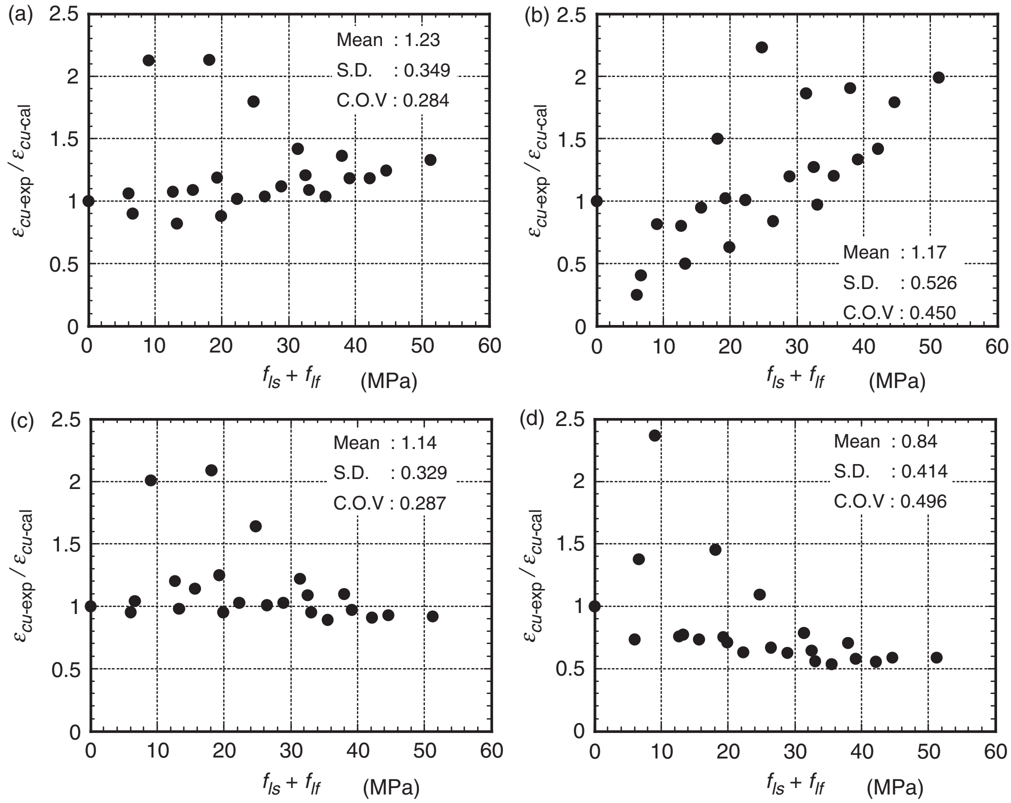

Figure 11. *Comparison between experimental and predicted maximum axial strains: (a) Mander et al., (b) Mirmiran et al., (c) Lam and Teng, and (d) Saafi et al.*

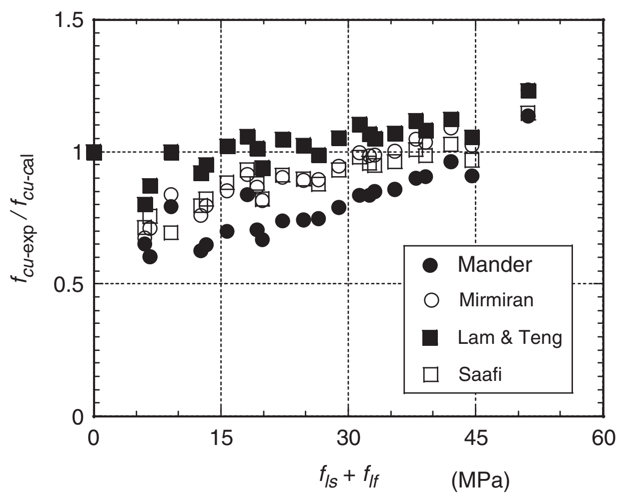

Figure 12. *Comparison between experimental and predicted compressive strengths.*

Proposed Model for Concrete Confined With Steel Spirals and FRP Sheets

The results discussed in the previous section indicate that the existing models developed for concrete confined with a single material (steel spirals or FRP composites) are unsuitable to predict the strength and corresponding strain for concrete confined with mixed materials (both steel spirals and FRP composites) because the models were originally developed to predict the behavior of concrete confined with single material. Thus, in this section, a new set of empirical equations is proposed for concrete confined with both steel spirals and FRP composites. The proposed empirical formulae are given below Equations (4)–(6), and Figure 13 presents a plot of the prediction curve.

$$f_c = E_c \cdot \varepsilon_c + (f'_c - E_c \cdot \varepsilon_{c0})\left(\frac{\varepsilon_c}{\varepsilon_{c0}}\right)^2 \quad \text{for} \quad 0 < \varepsilon_c \le \varepsilon_{c0} \tag{4a}$$

$$f_c = f'_c + (f_{cs} - f'_c)\left(\frac{\varepsilon_c - \varepsilon_{c0}}{\varepsilon_{cs} - \varepsilon_{c0}}\right)^{0.7} \quad \text{for} \quad \varepsilon_{c0} < \varepsilon_c \le \varepsilon_{cs} \tag{4b}$$

$$f_c = f_{cs} + (f_{cu} - f_{cs})\left(\frac{\varepsilon_c - \varepsilon_{cs}}{\varepsilon_{cu} - \varepsilon_{cs}}\right)^{0.7} \quad \text{for} \quad \varepsilon_{cs} < \varepsilon_c \le \varepsilon_{cu}, \tag{4c}$$

where $E_c = 4700\sqrt{f'_c}$ (MPa)

$$\varepsilon_{cs} = \varepsilon_{cu}\left\{0.85 + 0.03 \cdot \left(\frac{f_{lf}}{f_{ls}}\right)\right\} \text{ and } f_{cs} = 0.95 \cdot f_{cu} \quad \text{for} \quad f_{lf} \ge f_{ls}$$

$$\varepsilon_{cs} = 0.7 \cdot \varepsilon_{cu} \quad \text{and} \quad f_{cs} = (\varepsilon_{cs}/\varepsilon_{cu})^{0.40} \cdot f_{cu} \quad \text{for} \quad f_{lf} < f_{ls}$$

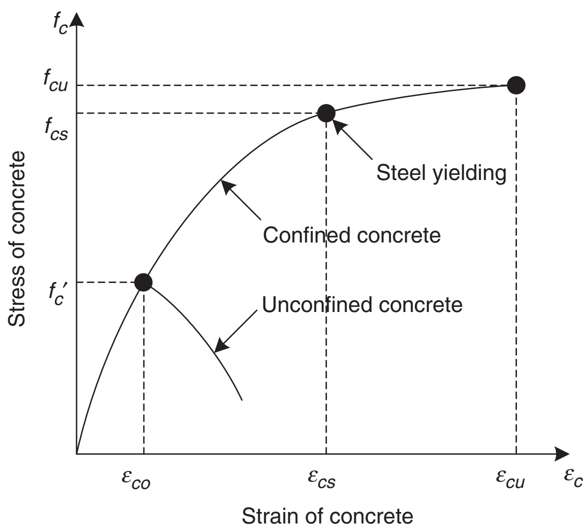

Figure 13. *Stress–strain model of concrete confined with steel spiral and FRP composites.*

The proposed empirical model consists of three equations. The first one is the unconfined concrete model [37] to predict the stress–strain curve up to $\varepsilon = \varepsilon_{c0}$, which corresponds to the peak stress (f'_c) of unconfined concrete. The second and the third equations are obtained by adjusting the exponents of the confined concrete model by Muguruma et al. [37] to predict the stress–strain curves of the tested confined concrete cylinders for the strain ranging from the ε_{c0} to $\varepsilon_{cs,}$ and from ε_{cs} to ε_{cu}, respectively. It is noted that the curves constructed by the proposed equations are continuous pointwise only. However, the proposed equations can provide resonable approximations for the cases in which the smoothness of the stress–strain curve is not an absolute requirement, as demonstrated in Figures 9 and 10. The variables ε_{c0}, ε_{cs}, and ε_{cu} are the concrete strain at the peak unconfined concrete stress (f'_c), the confined concrete strain at the onset of yielding in the transverse steel (corresponding to a concrete confined stress of f_{cs}), and the concrete strain at the confined peak stress (f_{cu}), respectively.

The ways to determine the two remaining values for the proposed model (the maximum confined compressive strength, f_{cu}, and the ultimate concrete strain, ε_{cu}) are proposed as the following. To estimate f_{cu}, Equation (5) proposed by Lam and Teng [34] is adopted since the equation produces satisfactory estimates, as discussed earlier and shown in Figure 12.

$$f_{cu} = f'_c\left(1 + 2\frac{f_l}{f'_c}\right) \tag{5}$$

Similarly, to estimate the ultimate concrete strain, ε_{cu}, Lam and Teng model [34] is modified, based on the test results of this study by the introduction of two new parameters, k_s and k_f, as given in Equation (6):

$$\varepsilon_{cu} = \varepsilon_{co}\left(1.75 + 5.25\left(\frac{k_f \cdot f_{lf} + k_s \cdot f_{ls}}{f'_c}\right)\left(\frac{\varepsilon_{frp,r}}{\varepsilon_{co}}\right)^{0.45}\right), \tag{6}$$

where $k_s = (2 - f_{lf}/f_{ls})$ and $k_f = 1$ for $f_{lf} \leq f_{ls}$

$k_s = 1$ and $k_f = 1$ for $f_{lf} > f_{ls}$

$\varepsilon_{frp,r}$ = rupture strain of FRP

Figure 14 shows the ratios of the predicted values of ε_{cu}, ε_{cs}, and f_{cs} to the experimental values. Note that the number of points in Figure 14(b) and (c) is one less than that in Figure 14(a) because the steel strain measurement of S4F1 could not be recorded while performing the test. For the test results obtained in this study, the predicted values show good agreement with the experimental results. The improvement from the existing model to the proposed model can also be seen in Figures 9(b) and 10, which show more accurate softening behavior of the concrete after the yielding of the steel spirals. Table 4 gives the ratios of the experimental maximum concrete compressive stress and corresponding axial strain of each specimen to their predicted values obtained from the four existing models considered in this study.

It is noted that the validity of the proposed model needs to be verified against more independent experimental data, though most of the test data available in the literature is from FRP-wrapped reinforced concrete column tests, in which the columns are subjected to both axial and bending loads rather than a pure axial load. Hence, the comparisons reported here are limited to those obtained from the current study. More elaborate parametric studies to improve the model are planned for future research.

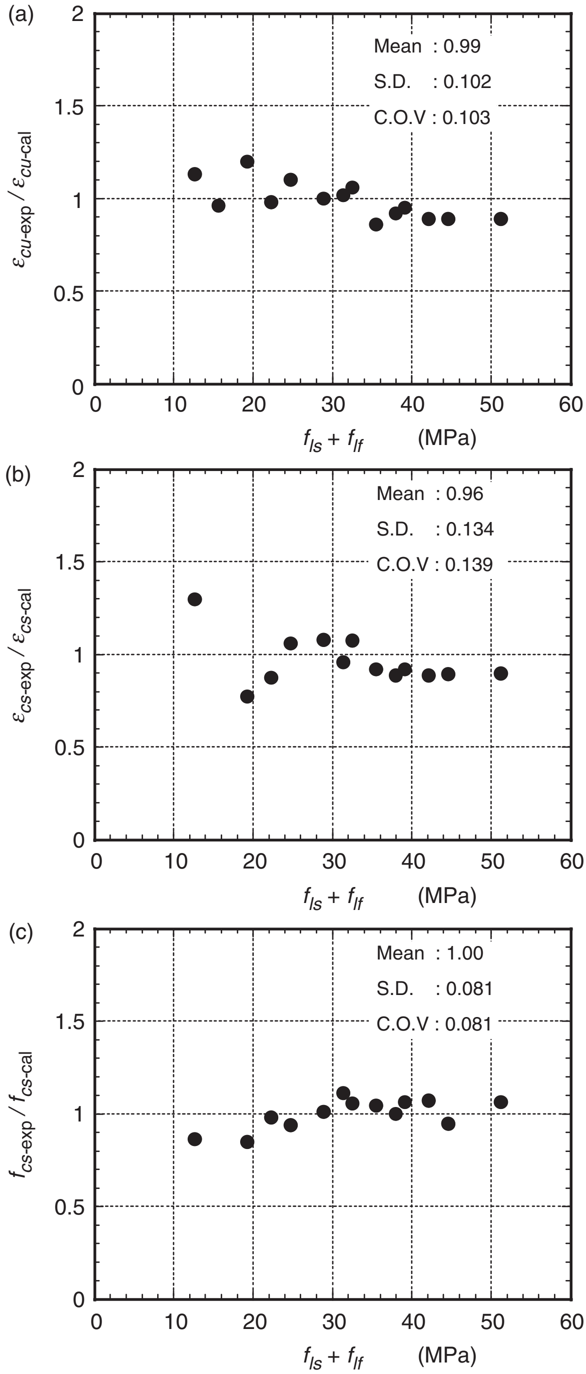

Figure 14. *Comparison between experimental and predicted using the proposed equation: (a) maximum axial strains, (b) axial strain at steel yielding, and (c) compressive stress at steel yielding.*

Table 4. Comparison between the experimental and the predicted strengths and corresponding strains (only those specimens with the mixed confinement).

Specimens	f_{cu}−exp (MPa)	ε_{cu}−exp	$\frac{f_{cu-exp}}{f_{cu-man}}$	$\frac{f_{cu-exp}}{f_{cu-mir}}$	$\frac{f_{cu-exp}}{f_{cu-sa}}$	$\frac{f_{cu-exp}}{Eq.(5)}$	$\frac{\varepsilon_{cu-exp}}{\varepsilon_{cu-man}}$	$\frac{\varepsilon_{cu-exp}}{\varepsilon_{cu-mir}}$	$\frac{\varepsilon_{cu-exp}}{\varepsilon_{cu-lam}}$	$\frac{\varepsilon_{cu-exp}}{\varepsilon_{cu-sa}}$	$\frac{\varepsilon_{cu-exp}}{Eq.(6)}$
S6F1	50.4	0.017	0.63	0.76	0.79	0.84	1.07	0.80	1.20	0.76	1.13
S6F2	68.5	0.025	0.70	0.86	0.88	0.94	1.19	1.02	1.25	0.75	1.20
S6F4	99.5	0.034	0.84	0.99	0.96	1.00	1.21	1.27	1.09	0.64	1.06
S6F5	114.6	0.036	0.91	1.04	0.98	1.02	1.18	1.33	0.97	0.58	0.95
S4F1	60.0	0.019	0.70	0.85	0.88	0.92	1.09	0.95	1.14	0.73	0.96
S4F2	74.8	0.023	0.74	0.90	0.91	0.95	1.02	1.01	1.03	0.63	0.98
S4F3	88.8	0.029	0.79	0.95	0.93	0.97	1.12	1.20	1.03	0.63	1.00
S4F4	104.2	0.030	0.86	1.00	0.96	0.99	1.04	1.20	0.89	0.54	0.86
S4F5	123.6	0.036	0.96	1.09	1.03	1.05	1.19	1.42	0.91	0.55	0.89
S2F1	72.9	0.039	0.74	0.89	0.90	0.90	1.79	2.23	1.64	1.09	1.10
S2F2	92.7	0.036	0.84	1.00	0.98	0.98	1.42	1.86	1.22	0.79	1.02
S2F3	108.0	0.034	0.90	1.05	1.01	1.01	1.36	1.90	1.10	0.71	0.92
S2F4	115.7	0.038	0.90	1.02	0.97	0.96	1.24	1.79	0.93	0.59	0.89
S2F5	150.8	0.043	1.13	1.23	1.15	1.13	1.33	1.99	0.92	0.59	0.89
Ave			0.83	0.97	0.95	0.97	1.23	1.43	1.09	0.68	0.99
COV			15.5%	12.1%	8.8%	7.0%	16.2%	31.4%	18.1%	20.8%	10.3%

$f_{cu-\exp}$ = ultimate compressive strength of the tested cylinders; f_{cu-man}, f_{cu-mir}, and f_{cu-sa} = ultimate compressive strength calculated by equations in Table 3; $\varepsilon_{cu-\exp}$ = compressive strain corresponding to $f_{cu-\exp}$ of the tested cylinders; ε_{cu-man}, ε_{cu-mir}, ε_{cu-lam}, and ε_{cu-sa} = compressive strain corresponding to ultimate compressive strength calculated by equations in Table 3; COV = coefficient of variation.

CONCLUSIONS

The compressive response of concrete confined with both FRP composites and a steel spiral is studied experimentally and analytically in this research. Based on the experimental results of this study, the following conclusions are made:

(1) For a given steel spiral volumetric ratio, the ultimate compressive strength of concrete increases almost linearly with the thickness of the FRP. However, the trend is not as prominent in the corresponding axial strain, which shows a scatter as the number of FRP wraps increases.
(2) In the stress–strain curve of concrete, when the compressive stress of FRP steel–confined concrete is less than or equal to the unconfined compressive strength of concrete, the behavior of the confined concrete is identical to that of unconfined concrete. However, once the compressive stress exceeds the strength of unconfined concrete, the concrete exhibits behavior that lies between that of concrete confined with steel spiral only and that of concrete confined with FRP only.
(3) The results show that the increase in strength (Δf_{s+f}) achieved by the two confining materials can be conservatively obtained by summing the increments of the strength of two companion cylinders that are each confined with a different material. That is, $\Delta f_{s+f} = \Delta f_s + \Delta f_f$.
(4) The results show that the axial strain corresponding to the peak compressive stress of a concrete cylinder confined with two materials (i.e., steel spirals and FRP wraps) can be approximated as the peak strain of a companion concrete cylinder confined with only one material of which the confining stress is equal to the weighted total confining stress of the two materials.

(5) A set of empirical equations is proposed to predict the compressive response of concrete confined with both FRP composites and steel spirals. The proposed equations predict the stress–strain curves of the cylinders, the peak stress, and the corresponding axial strain more accurately than the four existing models. However, further verification and improvement of the proposed model is necessary to accommodate various concrete design parameters.

NOMENCLATURE

A_{core}, A_{cover} = Cross-sectional areas of core and cover concretes, respectively
A_g = Gross cross-sectional area of cylinder
A_{sp} = Cross-sectional area of steel spiral
D = Diameter of concrete cylinder
d_s = Distance between the centers of the spiral
E_c = Modulus of elasticity of concrete
E_{frp} = Modulus of elasticity of FRP
f_c = Compressive axial stress
f'_c = Compressive strength of unconfined concrete
$f_{c\text{-core}}$ = Core concrete stress confined by both FRP and steel spiral
$f_{c\text{-cover}}$ = Cover concrete stress confined only by FRP
f_{cs} = Comprssive stress of confined concrete at yielding of steel spiral
f_{cu} = Compressive strength of confined concrete
f_{fy} = Tensile strength of the FRP
f_l = Total lateral confining pressure
f_{lf}, f_{ls} = Lateral confining pressures of FRP and steel spiral, respectively
f_{sy} = Yield strength of steel spiral
s = Pitch of spirals
t = Thickness of FRP
ε_c = Compressive strain of concrete
ε_{c0} = Compressive strain of unconfined concrete at peak stress
ε_{cs} = Compressive strain of confined concrete at yielding of steel spiral
ε_{cu} = Compressive strain at peak compressive stress
$\varepsilon_{\mathrm{frp},r}$ = Tensile rupture strain of FRP
ε_l = Lateral strain of specimen
Δf_s = Increase of strength due to confining of steel spiral
Δf_f = Increase of strength due to confining of FRP
Δf_{s+f} = Increase of strength due to confining of steel spiral and FRP ($= \Delta f_s + \Delta f_f$)

ACKNOWLEDGEMENTS

This work was supported by the Korea Research Foundation Grant funded by the Korean Government (MOEHRD) (KRF-D00845-I01622) and by the Basic Research Program of the Korea Science & Eng. Foundation (Grant No. R0A-2006-000-10234-0).

REFERENCES

1. Nishizaki, I., Takeda, N., Ishizuka, Y. and Shimomura, T. (2006). A Case Study of Life Cycle Cost Based on a Real FRP Bridge, In: *Proceedings of the Third International Conference on FRP Composites in Civil Engineering* (CICE2006), Miami, Florida, USA, pp. 99–102.
2. Ahmad, S.M. and Shah, S.P. (1982). Stress-Strain Curves of Concrete Confined by Spiral Reinforcement, *ACI Structural Journal*, **79**(6): 484–490.
3. Mander, J.B., Priestley, M.J.N. and Park, R. (1988). Observed Stress Strain Behavior of Confined Concrete, *ASCE Journal of Structural Engineering*, **114**(8): 1827–1849.
4. Kurt, C.E. (1978). Concrete Filled Structural Plastic Columns, *Journal of Structural Division ASCE*, **104**(1): 55–63.
5. Fardis, M.N. and Khalili, H. (1981). Concrete Encased in Fiberglass-Reinforced Plastic, *Journal of American Concrete Institution Proceedings*, **78**(6): 440–446.
6. Fardis, M.N. and Khalili, H. (1982). FRP-Encased Concrete as a Structural Material, *Magazine Concrete Research*, **34**(121): 191–202.
7. Ahmad, S.M., Khaloo, A.R. and Irshaid, A. (1991). Behavior of Concrete Spirally Confined by Fiberglass Filaments, *Magazine Concrete Research*, **43**(156): 143–148.
8. Nanni, A. and Bradford, N.M. (1995). FRP Jacketed Concrete Under Uniaxial Compression, *Construction Building Material*, **9**(2): 115–124.
9. Harmon, T.G. and Slattery, K.T. (1992). Advanced Composite Confinement of Concrete, In: *1st International Conference on Advanced Composite Materials in Bridges and Structures*, Sherbrooke, Quebec, Canada, pp. 299–306.
10. Picher, F., Rochette, P. and Labossiere, P. (1996). Confinement of Concrete Cylinders with CFRP, In: *Proceedings of the ICCI'96*, Tuscon, Arizona, pp. 829–841.
11. Watanabe, K., Nakamura, H., Honda, Y., Toyoshima, M., Isao, M., Fujimaki, T., Kaneto, M. and Shirai, N. (1997). Confinement Effect of FRP Sheet on Strength and Ductility of Concrete Cylinders Under Uniaxial Compression, In: *Proceedings of the FRPRCS-3*, Sapporo, Japan, Vol. 1, pp. 233–240.
12. Miyauchi, K., Nishibayashi, S. and Inoue, S. (1997). Estimation of Strengthening Effects with Carbon Fiber Sheet for Concrete Column, In: *Proceedings of the FRPRCS-3*, Sapporo, Japan, Vol. 1, pp. 217–224.
13. Kono, S., Inazumi, M. and Kaku, T. (1998). Evaluation of Confining Effects of CFRP Sheets on Reinforced Concrete Members, In: *Proceedings of the ICCI'98*, Tuscon, Arizona, pp. 343–355.
14. Toutanji, H. (1999). Stress-Strain Characteristics of Concrete Columns Externally Confined with Advanced Fiber Composites Sheets, *ACI Materials Journal*, **96**(3): 397–404.
15. Matthys, S., Taerwe, L. and Audenaert, K. (1999). Tests on Axially Loaded Concrete Columns Confined by Fiber Reinforced Polymer Sheet Wrapping, In: *Proceedings of the FRPRCS-4*, Baltimore, pp. 217–228.
16. Shahawy, M., Mirmiran, A. and Beitelmann, T. (2000). Tests and Modeling of Carbon Wrapped Concrete Columns, *Composites Part B*, **31**(6–7): 471–480.
17. Rochette, P. and Labossiere, P. (2000). Axial Testing of Rectangular Column Models Confined with Composites, *Journal of Composites for Construction, ASCE*, **4**(3): 129–136.
18. Micelli, F., Myers, J.J. and Murthy, S. (2001). Effect of Environmental Cycles on Concrete Cylinders Confined with FRP, In: *Proceedings of the CCC2001 International Conference on Composites in Construction*, Porto, Portugal.
19. Rousakis, T. (2001). Experimental Investigation of Concrete Cylinders Confined by Carbon FRP Sheets, Under Monotonic and Cyclic Axial Compressive Load. Research Report, Chalmers University of Technology, Goteborg, Sweden.
20. Mirmiran, A. and Shahawy, M. (1997). Behavior of Concrete Columns Confined by Fiber Composites, *ASCE Journal of Structural Engineering*, **123**(5): 583–590.
21. Saafi, M., Toutanji, H.A. and Li, Z. (1999). Behavior of Concrete Columns Confined with Fiber Reinforced Polymer Tubes, *ACI Materials Journal*, **96**(4): 500–509.

22. La Tegola, A. and Manni, O. (1999). Experimental Investigation on Concrete Confined by Fiber Reinforced Polymer and Comparison with Theoretical Model, In: *Proceedings of the FRPRCS-4*, Baltimore.
23. Fam, A.Z. and Rizkalla, S.H. (2001). Behavior of Axially Loaded Concrete-filled Circular Fiber-reinforced Polymer Tubes, *ACI Structural Journal*, **98**(3): 280–289.
24. Saadatmanesh, H., Ehsani, M.R. and Li, M.W. (1994). Strength and Ductility of Concrete Columns Externally Reinforced with Fiber Composite Straps, *ACI Structural Journal*, **91**(4): 434–447.
25. Mirmiran, A. and Shahawy, M. (1996). A New Concrete-filled Hollow FRP Composite Column, *Composites Part B*, **27**(3–4): 263–268.
26. Samaan, M., Mirmiran, A. and Shahawy, M. (1998). Model of Concrete Confined by Fiber Composites, *ASCE Journal of Structural Engineering*, **124**(9): 1025–1031.
27. Spoelstr, M.R. and Monti, G. (1999). FRP-confined Concrete Model, *Journal of Composites for Construction, ASCE*, **3**(3): 143–150.
28. Teng, J.G. and Lam, L. (2004). Behavior and Modelling of FRP-confined Concrete, *ASCE Journal of Structural Engineering*, **130**(11): 1713–1723.
29. Lee, J.-Y., Yi, C.-K. and Oh, Y.-J. (2008). Strengthening of Concrete with Mixed Confinement Materials – Steel Hoops and FRP Composites, *Science and Engineering of Composites*, **15**(1): 1–19.
30. Liu, H.-K., Tai, N.-H. and Chen, C.-C. (2000). Compression Strength of Concrete Columns Reinforced by Non-adhesive Filament Wound Hybrid Composites, *Composites: Part A*, **31**(3): 221–233.
31. Lam, L. and Teng, J.G. (2004). Ultimate Condition of FRP-confined Concrete, *Journal of Composites for Construction, ASCE*, **8**(6): 539–548.
32. Mander, J.B., Priestley, M.J.N. and Park, R. (1988). Theoretical Stress-Strain Model for Confined Concrete, *ASCE Journal of Structural Engineering*, **114**(8): 1804–1826.
33. Samman, M., Mirmiran, A. and Shahawy, M. (1998). Model of Concrete by Fiber Composites, *ASCE Journal of Structural Engineering*, **124**(9): 1025–1031.
34. Lam, L. and Teng, J.G. (2003). Design-oriented Stress-Strain Model for FRP-Confined Concrete, *Construction and Building Materials*, **17**: 471–489.
35. Popovics, S. (1973). A Numerical Approach to the Complete Stress-Strain Curve of Concrete, *Cement and Concrete Research*, **3**(5): 583–599.
36. Elwi, A.A. and Murray, D.W. (1979). A 3D Hypoelastic Concrete Constitutive Relationship, *ASCE Journal of Engineering Mechanics Division*, **105**(4): 623–641.
37. Muguruma, H., Watanabe, F., Iwashizmiu, T. and Mitsueda, R. (1983). Ductility Improvement of High Strength Concrete by Lateral Confinement, *Transactions of Japan Concrete Institute*, **5**: 403–410.